Biomaterials 129 (2017) 152–162

Contents lists available at ScienceDirect

Biomaterials

journal homepage: www.elsevier.com/locate/biomaterials

Improvement of paracellular transport in the Caco-2 drug screening model using protein-engineered substrates

Rebecca L. DiMarco [a, 1], Daniel R. Hunt [b, 1], Ruby E. Dewi [c], Sarah C. Heilshorn [c, *]

[a] Department of Bioengineering, Stanford University, Stanford, CA, USA
[b] Department of Chemical Engineering, Stanford University, Stanford, CA, USA
[c] Department of Materials Science and Engineering, Stanford University, Stanford, CA, USA

ARTICLE INFO

Article history:
Received 14 December 2016
Received in revised form
1 March 2017
Accepted 14 March 2017
Available online 18 March 2017

Keywords:
Caco-2
Paracellular
Tight junction
Extracellular matrix
Protein engineering

ABSTRACT

The Caco-2 assay has achieved wide popularity among pharmaceutical companies in the past two decades as an *in vitro* method for estimation of *in vivo* oral bioavailability of pharmaceutical compounds during preclinical characterization. Despite its popularity, this assay suffers from a severe underprediction of the transport of drugs which are absorbed paracellularly, that is, which pass through the cell-cell tight junctions of the absorptive cells of the small intestine. Here, we propose that simply replacing the collagen I matrix employed in the standard Caco-2 assay with an engineered matrix, we can control cell morphology and hence regulate the cell-cell junctions that dictate paracellular transport. Specifically, we use a biomimetic engineered extracellular matrix (eECM) that contains modular protein domains derived from two ECM proteins found in the small intestine, fibronectin and elastin. This eECM allows us to independently tune the density of cell-adhesive RGD ligands presented to Caco-2 cells as well as the mechanical stiffness of the eECM. We observe that lower amounts of RGD ligand presentation as well as decreased matrix stiffness results in Caco-2 morphologies that more closely resemble primary small intestinal epithelial cells than Caco-2 cells cultured on collagen. Additionally, these matrices result in Caco-2 monolayers with decreased recruitment of actin to the apical junctional complex and increased expression of claudin-2, a tight junction protein associated with higher paracellular permeability that is highly expressed throughout the small intestine. Consistent with these morphological differences, drugs known to be paracellularly transported *in vivo* exhibited significantly improved transport rates in this modified Caco-2 model. As expected, permeability of transcellularly transported drugs remained unaffected. Thus, we have demonstrated a method of improving the physiological accuracy of the Caco-2 assay that could be readily adopted by pharmaceutical companies without major changes to their current testing protocols.

© 2017 Elsevier Ltd. All rights reserved.

1. Introduction

Oral drug administration is the most commonly used route because it's safe, convenient, inexpensive, and associated with high patient compliance [1]. In order to be physiologically effective, orally administered drugs must first be absorbed by the body, a process which occurs largely in the small intestines [2,3].

Various cellular assays, including the Caco-2 and Madin-Darby Canine Kidney (MDCK) models, have been developed to serve as *in vitro* models of drug absorption across the healthy small intestinal epithelium [4,5]. The MDCK model suffers from generally low metabolic enzyme activity and transport protein expression [6]. Most notably, MDCK cells greatly under-express P-glycoprotein, a key efflux transport molecule that exists in the plasma membrane of healthy intestinal epithelium and targets drugs to be exported rather than absorbed [7,8]. As such, the most widely used *in vitro* assay to predict the absorption of these drugs is the Caco-2 assay, in which an immortalized human colorectal adenocarcinoma-derived cell line is cultured to confluence on a collagen type-I matrix to model the epithelial lining of the small intestine (Fig. 1a) [9,10]. This assay has been extensively adopted by the pharmaceutical industry due to its ease of use and ability to model the absorption of a variety of compounds [11]. Despite its

* Corresponding author. Materials Science and Engineering Dept, 476 Lomita Mall, McCullough Room 246, Stanford University, Stanford, CA, 94305-4045, USA.
E-mail address: heilshorn@stanford.edu (S.C. Heilshorn).
[1] These authors contributed equally to this work.

http://dx.doi.org/10.1016/j.biomaterials.2017.03.023
0142-9612/© 2017 Elsevier Ltd. All rights reserved.

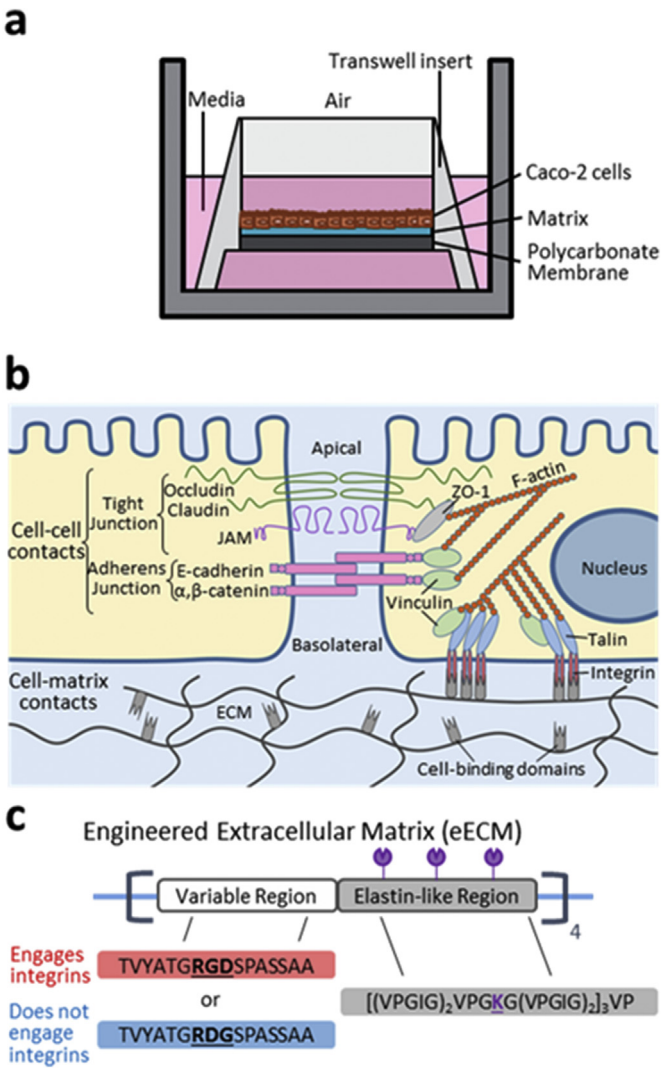

Fig. 1. Schematic of proposed assay to improve paracellular transport for *in vitro* drug screening. (a) Schematic of the Caco-2 monolayer assay in which drug molecules are added to the apical side and their transport to the basolateral side is monitored over time to predict intestinal absorption. (b) Schematic of key cell-cell and cell-matrix interactions that contribute to regulation of paracellular transport through tight junctions that connect neighboring cells. (c) Schematic representation and amino acid sequences of the engineered extracellular matrices (eECMs) used to replace the traditional collagen I matrix in the standard Caco-2 monolayer assay.

prevalence of use, the Caco-2 assay suffers from several shortcomings that limit its physiological accuracy, including atypical mucous production and altered expression of metabolizing enzymes and transport proteins relative to healthy small intestine. Another notable shortcoming of the Caco-2 assay is the significant under-prediction of paracellular absorption, the transport of molecules through tight junctions that connect neighboring cells [10,12,13]. Thus, continued reliance on the Caco-2 assay may result in the rejection of otherwise promising paracellularly transported drug candidates due to artificially poor pharmacokinetic parameters. For example, one of the most commonly prescribed medications worldwide, the paracellularly-absorbed drug ranitidine (Zantac®) was developed before the widespread use of the Caco-2 assay, which incorrectly predicts little to no absorption of this drug [10,14,15].

To address this major limitation, many groups have proposed modified Caco-2 assays to improve its ability to accurately predict *in vivo* biocompatibility via enhanced paracellular transport rate. Typically, these rely on addition of chemicals [16–20] or co-culture with other cell types [12,21–24]. Various three-dimensional (3D) drug screening models have also been developed, including organoid structures derived from primary tissue [25,26] and microfluidic, organ-on-a-chip devices [27]. While scientifically interesting, these strategies are technically cumbersome and not readily translatable to high-throughput settings. Here, we propose an alternative strategy to enhancing Caco-2 paracellular transport by simply modifying the matrix on which the cells are cultured. We hypothesize that modifying cell-matrix contacts will alter the actin cytoskeleton, which will influence cell-cell contacts and hence modulate paracellular transport through intercellular tight junctions. Previous studies have shown that focal adhesions, which can be formed at cell-matrix contact points, influence the development and maintenance of tight junctions through the actin cytoskeleton [28–31]. For example, inhibiting FAK expression or phosphorylation results in decreased barrier function and increased paracellular transport [28]. Additionally, both β1 and β2 subunits of integrins, the transcellular membrane receptors that directly bind to extracellular matrices, have been shown to affect paracellular permeability [32]. Further, disruption of the actin cytoskeleton, known to be regulated by cell-matrix contacts, through the use of small molecule inhibitors of actin polymerization [31] or inhibitors of its upstream effectors myosin light chain kinase (MLCK) [33] and the Rho family of GTP-ases [34,35] has been shown to affect epithelial barrier function.

These data suggest that replacing the standard collagen type I with an alternative, engineered matrix that differentially engages Caco-2 cells is a viable biomaterial approach to modify intercellular tight junctions and regulate paracellular transport. In this work, we utilize in parallel two biomaterials strategies commonly used to influence cell-matrix interactions: modulation of cell-binding domain (CBD) density and tuning of extracellular matrix (ECM) stiffness. Both material properties are known to influence actin cytoskeletal organization and cell spreading [36–39], and we hypothesize that in turn, they will regulate intercellular contacts and paracellular transport (Fig. 1b).

Here, we use a well-characterized and tunable engineered extracellular matrix (eECM) to prove our hypothesis. This eECM is modular in structure, comprising an elastin-like region for control of mechanical properties and, separately, a variable region comprised either of an integrin-engaging sequence or a non-integrin-engaging sequence (Fig. 1c). Expressed as recombinant proteins from genetically encoded plasmids, the eECM's biochemical and biomechanical properties can be tuned independently. With these properties, this eECM allows us to study the effects of CBD density and matrix stiffness, both separately and in combination, on Caco-2 barrier function.

Several methods exist to assess endothelial/epithelial cell monolayer confluence and barrier quality, including determination of fluid filtration coefficient (K_f), hydraulic conductivity (L_p), apparent solute permeability (P_{app}), and transepithelial electrical resistance (TEER) [40,41]. In our work, we have selected to measure the apparent solute permeability (P_{app}) through a drug transport assay, as it is the most direct measurement for evaluating our variable of interest: the permeability of the Caco-2 monolayer to paracellularly transported drugs [42].

We demonstrate that both CBD density and matrix stiffness independently and synergistically affect the paracellular permeability of mature Caco-2 monolayers, with improved permeability observed on cells cultured on matrices of lower CBD density and less mechanical stiffness.

2. Results and discussion

2.1. Engineered extracellular matrix (eECM) for Caco-2 monolayer culture

Driven by our hypothesis that modulating cell-matrix interactions will influence cell-cell contacts, we replaced the adsorbed collagen type I matrix used in the standard Caco-2 assay with recombinant eECMs to enhance paracellular transport in mature Caco-2 monolayers. Using recombinant protein-engineering techniques, we synthesized modular eECM materials containing domains derived from natural ECM proteins found in healthy intestinal tissue [43,44]. Specifically, an amino acid sequence derived from fibronectin was alternated with an elastin-like amino acid sequence. We developed two alternative constructs, one version which contains the intact RGD amino acid sequence which is known to engage integrins, and another version where the RGD sequence has been permuted to RDG, a sequence which is known not to engage integrins [45,46]. Full amino acid sequences are provided in the Supplemental Information (Fig. S1a).

These modular eECMs allowed the independent tuning of both cell-binding domain (CBD) density and material stiffness, in order to decouple the potential effects of matrix biochemical and biomechanical cues on Caco-2 barrier function. CBD density was varied by simply blending the integrin-engaging eECM with the non-integrin-engaging eECM at a desired ratio. In parallel, eECM stiffness was varied by tuning the fabrication parameters for the eECM coatings. For a direct comparison to the traditional Caco-2 assay, where collagen I is physically adsorbed onto a polycarbonate membrane, an identical fabrication procedure was followed for the eECM. For these coatings, the cells were assumed to sense the stiffness of the underlying rigid membrane, 3.3 GPa [47]. As an alternative to better mimic the mechanical stiffness of the small intestinal submucosa (SIS) (~150–500 kPa) [48–50]. eECM coatings were also fabricated as crosslinked matrices. Specifically, the stiffness of these eECM coatings (thickness ~60 μm) was controlled by tuning the reactive group stoichiometric ratio between the eECM and the crosslinker tetrakis (hydroxymethyl) phosphonium chloride (THPC), which specifically reacted with lysine residues contained within the elastin-like structural region [51].

To determine the mechanical properties of crosslinked eECM coatings, atomic force microscopy (AFM) was utilized to determine the Young's modulus (E) in compression. For the studies presented here, eECM crosslinked coatings of 240 and 640 kPa were selected to bracket the average reported value of the stiffness of the SIS (Fig. S1B).

2.2. eECM CBD density and stiffness influence cell area in mature Caco-2 monolayers

To probe our hypothesis that changes in eECM properties would affect the cytoskeletal organization of Caco-2 cells, we first observed cell spreading within mature Caco-2 monolayers. As CBD was decreased (by decreasing the percentage of the matrix composed of integrin-engaging eECM) a tighter packing of cells was observed within the monolayer (as visualized by DAPI nuclear staining (Fig. 2a)), indicative of a decrease in cell spread area. This qualitative observation was confirmed by quantitative analysis of projected cell area (Fig. 2b, top panel).

The fibronectin-derived, integrin-engaging RGD sequence is commonly used to promote cell binding to biomaterials. This sequence is known to preferentially engage $\alpha_v\beta_3$ integrins as well as $\alpha_5/\alpha_v\beta_1$ integrins [45,52–55], which are both expressed by Caco-2 cells (Fig. S2). Collagen substrates, which are known to contain a myriad of CBDs, including RGD, resulted in the greatest amount of cell spreading. Compared to collagen substrates, which contain numerous different cell adhesion domains, the eECM with the highest CBD density ([RGD] ~12 pmol/cm^2, SI) resulted in significantly less cell spreading. Further decreasing the CBD density to 10% and 0% resulted in a further statistically significant ($P < 0.0001$) decrease in cell spread area (Fig. 2b, top). These results are consistent with previous literature showing that lower concentrations of CBD result in lower amounts of cell spreading in 2D [36–39,56].

Next, we evaluated the influence of matrix stiffness on cell spreading for mature Caco-2 monolayers. As expected, cells cultured on softer substrates exhibited significantly less ($P < 0.001$) cell spreading compared to cells cultured on substrates with the stiffness used in the standard Caco-2 assay (3.3 GPa) (Fig. 2b, bottom). This observation is consistent with previously published studies of 2D cell spreading [36–39]. Unsurprisingly, taking into account both variables of CBD density and matrix stiffness, the greatest difference to adsorbed collagen was observed in the monolayers cultured on eECM that has the lowest stiffness and the lowest CBD density, eECM (240 kPa, 0%).

To confirm these observations, scanning electron microscopy (SEM) micrographs of mature Caco-2 monolayers on eECM substrates were compared to those on collagen and an explant of primary normal intestinal tissue, both qualitatively (Fig. 2c) and quantitatively (Fig. 2d). Qualitatively, cells cultured on eECM substrates more closely resemble epithelial cells of healthy intestinal tissue when compared to those cultured on adsorbed collagen (Fig. 2c, top panels). To quantify these differences, masks of cell boundaries were generated from representative SEM micrographs of Caco-2 monolayers cultured on the various ECMs (Fig. 2c, bottom panels) and used to calculate average individual cell area. The result of this quantification further supports the improved similarity in projected cell area of cells cultured on eECM (240 kPa, 0%) to healthy intestinal tissue, when compared to those cultured on collagen or all other eECMs. Notably, despite these differences in cell spreading, Caco-2 cells cultured on all eECMs maintained proper apical-basolateral polarity as demonstrated by the apical-specific staining of the tight junction recruitment protein JAM-A (Fig. 2e). The polarized orientation of JAM-A with respect to the Caco-2 cell nuclei is observed across all conditions tested, including those of intermediate CBD density and stiffness (Fig. S3). To reach this final mature morphology, Caco-2 cells often undergo dynamic changes in cell spreading over time throughout the 28-day culture [10]. Cells cultured on adsorbed collagen substrates undergo a dramatic increase in cell area during the first few days of culture, after which cells regress to a much smaller size by 7 days of culture (Fig. S4). Interestingly, these dynamic changes in cell spreading are much less pronounced for all of the eECM coatings tested. Nevertheless, despite these changes in cell spreading phenotype over time, the final cell-spread area in the mature monolayers was found to be highly dependent on the underlying matrix upon which they are cultured (Fig. 2).

2.3. eECM CBD and stiffness influence paracellular transport and organization of actin cytoskeleton at apical junctional complex

To investigate if these observed differences in cell spreading correlate with changes in paracellular absorption, we measured the transport of the model paracellular drug fluorescein isothiocyanate (FITC)-labeled inulin (inulin-FITC) across monolayers cultured on various ECMs using the standard Caco-2 assay setup. Consistent with our hypothesis, our results show an inverse trend in paracellular absorption compared to that for cell spreading. Transport of inulin-FITC across Caco-2 monolayers is enhanced by decreasing

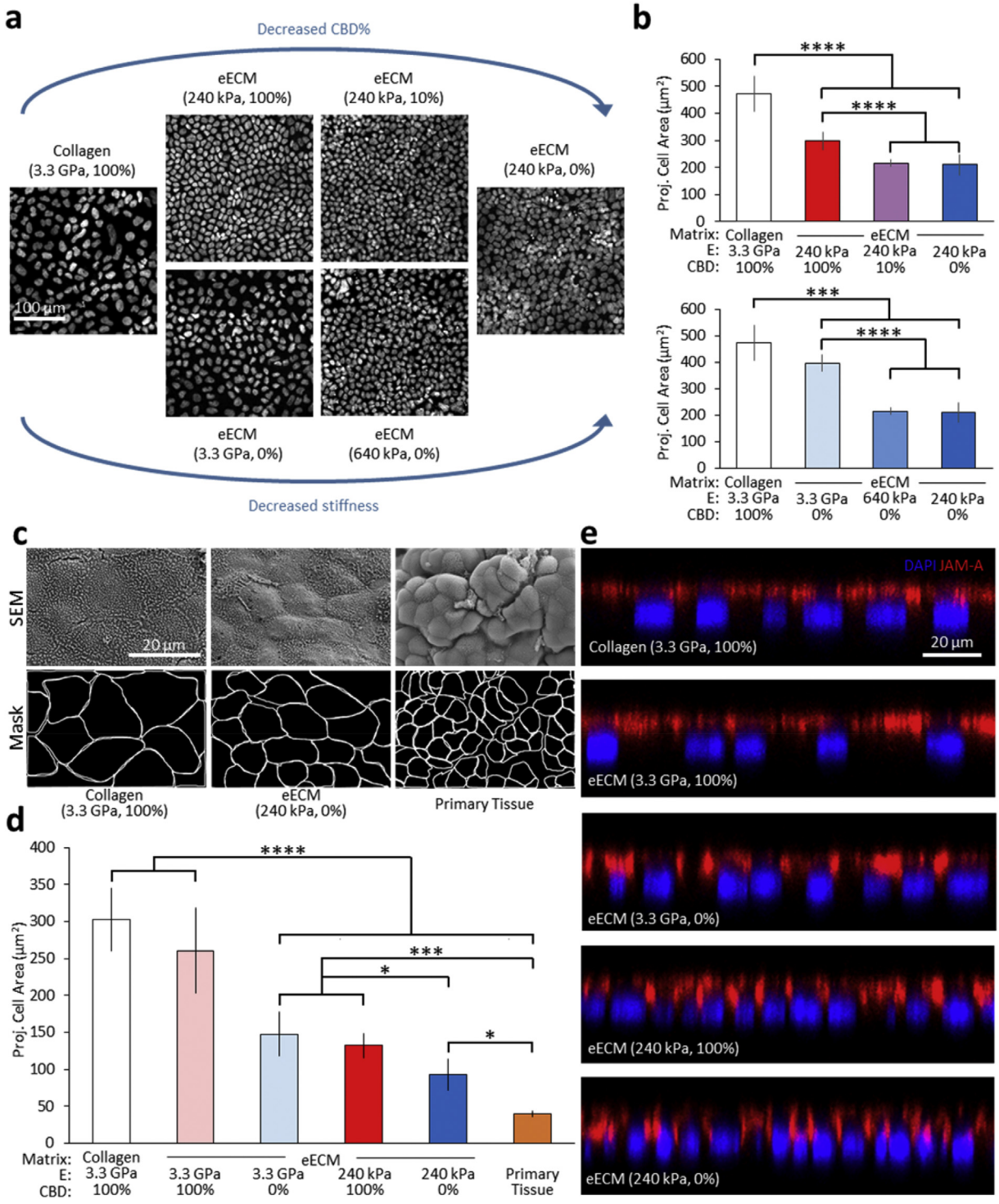

Fig. 2. eECM cell-binding domain (CBD) density and stiffness modulate the cell area of Caco-2 cells within mature monolayers. (a) Representative micrographs of DAPI-stained nuclei of Caco-2 monolayers demonstrating decreased cell area (and hence higher cell density) in monolayers cultured on eECM substrates with decreased CBD density or decreased stiffness. (b) Caco-2 projected cell area decreases when cultured on eECM with decreasing CBD density (top) and decreasing elastic modulus (E) (bottom). (c) Scanning electron microscopy (SEM) images and manual tracing of cell boundaries on representative matrices and explanted primary murine small intestinal tissue. (d) Quantification of SEM micrographs confirms that Caco-2 monolayers on eECM substrates with lower stiffness and fewer CBD have projected cell areas more similar to primary murine intestinal tissue compared to collagen I. (e) Cross-sectional z-stacks of Caco-2 monolayers on collagen and representative eECMs, stained for the tight junction protein JAM-A (red) and nuclei (blue), demonstrate the maintenance of proper cell polarity on all substrates and the presence of more columnar shaped cells on eECM of lower stiffness and fewer CBD. *$p < 0.05$, ***$p < 0.001$, ****$p < 0.0001$. (For interpretation of the references to colour in this figure legend, the reader is referred to the web version of this article.)

either CBD density (Fig. 3a) or mechanical stiffness (Fig. 3b) of our eECM films. Paracellular transport was most significantly enhanced on monolayers cultured on eECM (240 kPa, 10%) and (240 kPa, 0%), with measured P_{app} values of 2.2×10^{-6} and 1.6×10^{-6} cm s^{-1}, respectively, compared to those of monolayers cultured on the standard adsorbed collagen, 7.7×10^{-7} cm s^{-1}.

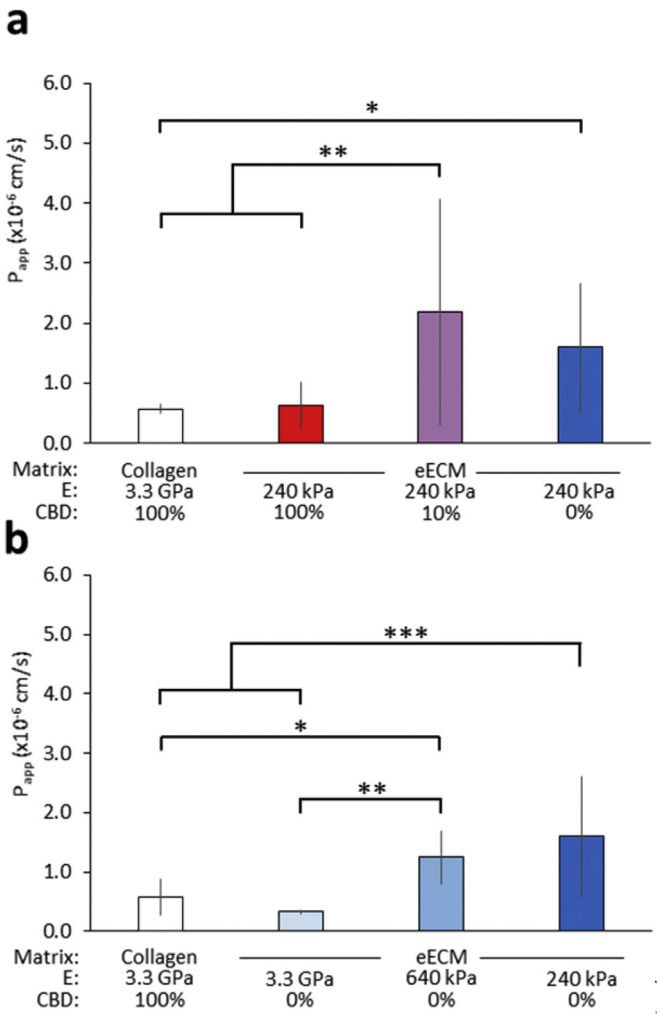

Fig. 3. Apparent permeability (P_{app}) of the model paracellular drug inulin-FITC. Caco-2 cells demonstrated enhanced P_{app} on eECM with (a) decreasing CBD density and (b) decreasing stiffness. *p < 0.05, **p < 0.01, ***p < 0.001.

Our data demonstrate that a synergistic effect of biomechanical and biochemical cues can be used to enhance paracellular transport across Caco-2 monolayers. Specifically, we have identified a plateau-like response in paracellular transport rates based on decreasing mechanical stiffness and decreasing interaction with cell-binding domains. Thus, there are saturation thresholds for both tunable substrate parameters beyond which further alteration (i.e. further decrease in stiffness or further decrease in the concentration of CBD) may no longer coincide with an increase in paracellular transport.

Significantly, all P_{app} values measured across experimental conditions were significantly lower than that of the acellular control, 5.7×10^{-5} cm s^{-1}, indicating the successful formation of confluent Caco-2 monolayers across all conditions tested after four weeks of culture.

These studies revealed an inverse correlation between paracellular transport and cell area with respect to changes in CBD density and matrix stiffness. This supports our hypothesis that changes in cell-matrix interactions can influence the organization of the actin cytoskeleton in Caco-2 cells, in turn affecting the properties of tight junctions that regulate the paracellular flux of molecules across the epithelial monolayer.

To further evaluate this hypothesis, we next examined the organization of the actin cytoskeleton as a function of changes in the CBD density and mechanical stiffness of the matrix (Fig. 4). Mature Caco-2 monolayers were stained with TRITC-phalloidin and visualized by confocal microscopy. Reconstructed cross-sectional xz-slices through the monolayers show actin accumulation at the basal surface for all substrates (Fig. 4a), again reinforcing the notion that all substrates supported proper apical-basolateral cell polarity. Single confocal xy slice images were taken at the apical junctional complex of the cells (Fig. 4b). Morphologically, actin localized at the apical side exhibited a highly junctional localization, with the cell-cell contacts outlined clearly in each condition [31,57]. Notably, the amount of actin that was localized to the apical junctional complex was decreased as a function of both CBD and eECM stiffness (Fig. 4c). These results are consistent with previous work that demonstrated an inverse correlation between the amount of actin that accumulates at cell-cell junctions and paracellular permeability [58,59].

2.4. eECM CBD and stiffness influence claudin-2 expression in mature Caco-2 monolayers

Having demonstrated that changes in eECM CBD density and stiffness affect the paracellular permeability and actin cytoskeletal organization, we then examined potential effects on the expression of tight junction proteins. We observed a dosage-responsive increase in the expression of the barrier-weakening, tight junction protein claudin-2 as a function of decreases in both CBD density and stiffness (Fig. 5 a,b). This increase in RNA expression of claudin-2, a protein that is expressed in 'leaky' epithelia and throughout the small intestine [60], is consistent with our permeability data (Fig. 3), which shows increases in FITC-inulin permeability on matrices with decreased CBD density and matrix stiffness. In contrast, only minor differences were observed in expression of the tight junction signaling protein JAM-A and barrier-tightening protein claudin-1. Additionally, we performed a 2-way analysis of variance (ANOVA) to assess the interaction between the two parameters of CBD density and matrix stiffness and found a synergistic effect for these two parameters in governing claudin-2 expression (P~0.001). A Tukey *post-hoc* test was applied to correct for multiple comparisons.

To confirm these findings, we used immunocytochemistry to fluorescently label and visualize the organization of the tight junction proteins claudin-2 and JAM-A by confocal microscopy (Fig. 5). Claudin-2 expression in mature Caco-2 monolayers was significantly more prominent on the eECM with the lowest CBD density and lowest stiffness (Fig. 5c and e), supporting the results obtained by RT-PCR. This evidence supports the idea that lower CBD density and decreased stiffness result in mature Caco-2 monolayers that have leakier tight junctions, as demonstrated by a higher level of claudin-2 at the RNA and protein levels. In contrast, no significant differences in JAM-A protein expression were observed across all conditions (Fig. 5d and f), recapitulating the results obtained by RT-PCR.

Caco-2 cells are known to require extended culture duration to differentiate and express absorptive enterocyte markers expressed by the small intestine [61]. Thus, we utilized RT-PCR to assay for changes in the expression of genes related to the small intestinal absorptive cell phenotype. Expression profiles of Caco-2 cells cultured on all eECM substrates closely resembled those on adsorbed collagen for markers of general epithelium (β-actin and E-cadherin) and intestinal epithelium (intestinal alkaline phosphatase). However, expression levels of small intestinal markers (the brush border enzymes sucrose-isomaltase and aminopeptidase) were significantly increased on eECM films with low stiffness and low CBD density (Fig. S5). These data suggest that extended culture

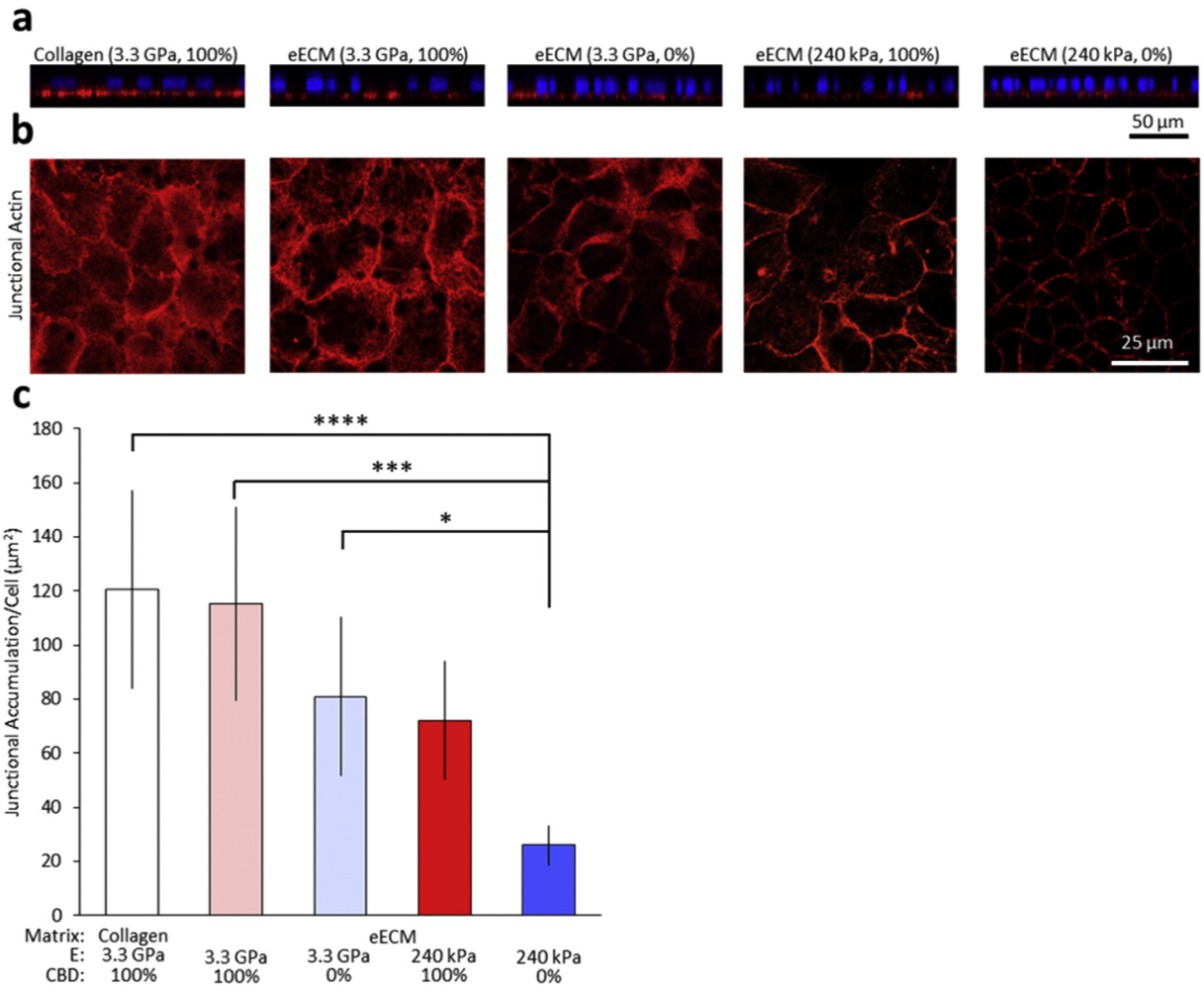

Fig. 4. Representative immunostaining of mature Caco-2 monolayers. (a) Orthogonal sections of Caco-2 monolayers on collagen and representative eECMs, stained with phalloidin (red) and DAPI (blue), demonstrate the maintenance of proper cell polarity on all substrates. (b) Confocal micrographs of immunostained samples for junctional actin (red) and with DAPI nuclear counterstain (blue). (c) Quantification of confocal micrographs show less junctional actin accumulation on eECM with decreased CBD density and decreased stiffness. $^{*}p < 0.05$, $^{**}p < 0.01$. (For interpretation of the references to colour in this figure legend, the reader is referred to the web version of this article.)

on our engineered substrate promotes the development of a more small intestinal enterocyte-like phenotype. Taken together, these results demonstrate that simply altering the properties of the biomaterial substrate may be an effective strategy to increase the activity of certain enzymes on the apical surface of epithelial absorptive cells. Additional investigation into the utilization of substrate properties to further improve Caco-2 model performance by altering mucus production, transporter protein expression, and metabolizing enzyme activity, are notable areas of interest for future work.

2.5. eECM CBD and stiffness effects on paracellular permeability to pharmaceutical drug molecules

Having demonstrated that Caco-2 morphology, apical actin accumulation, and claudin-2 expression could be controlled by changing the underlying biomaterial, we next set out to study the permeability of mature Caco-2 monolayers to several pharmaceutical drug molecules. We selected four compounds that are known to be transported predominantly via the paracellular pathway: histamine H2 receptor antagonists famotidine (Pepcid®) [62] and ranitidine (Zantac®) [62], and β-antagonists nadolol (Corgard®) [12] and atenolol (Tenormin®) [63]. We also selected two drug molecules that are known to be predominantly transported via transcellular routes: corticosteroid dexamethasone (Decadron®) [64] and non-steroidal anti-inflammatory drug naproxen (Aleve®) [65]. For 3 out of the 4 paracellularly transported compounds tested (ranitidine, nadolol, and atenolol), the P_{app} for cells on the eECM with decreased CBD and decreased stiffness was significantly higher compared to cells grown on collagen (Fig. 6). These data are consistent with our earlier experiments using the paracellular permeability reporter compound inulin-FITC (Fig. 3). As expected, no difference in permeability of the transcellularly transported drugs was observed across all biomaterial conditions (Fig. 6). These results suggest that the modifications to the underlying biomaterial specifically improve paracellular transport while not affecting other modes of drug transport.

The objective of the Caco-2 permeability assay for screening pharmaceutical compounds is to establish a predictive correlation between *in vitro* P_{app} with *in vivo* absorption. The results of Fig. 6 roughly recapitulate such a relationship. Transcellular compounds commonly have *in vivo* absorption availabilities that are greater than paracellular compounds. The transcellular compounds tested here, dexamethasone [64] and naproxen [66], have *in vivo* absorption of >85% and 99%, respectively, and their relative magnitude of absorption is recapitulated by the higher P_{app} value of

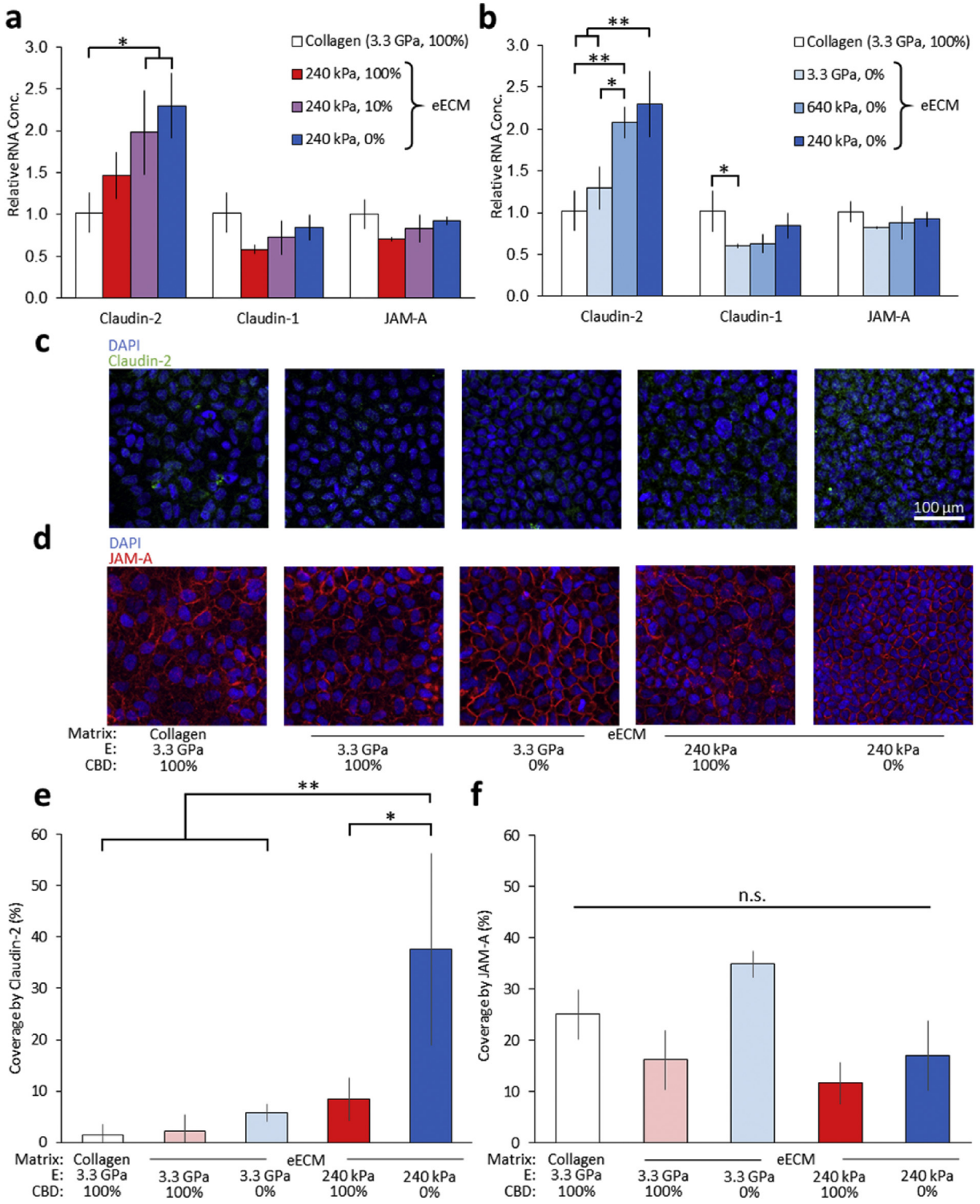

Fig. 5. Expression of barrier weakening protein claudin-2 is increased on substrates with decreased CBD density and decreased stiffness. (a,b) Relative mRNA expression levels of claudin-2 (barrier weakening), claudin-1 (barrier tightening), and JAM-A (recruitment) tight junction proteins on eECM with varying (a) CBD density and (b) stiffness. (c, d) Representative immunostaining of mature Caco-2 monolayers. Confocal micrographs of immunostained samples for (c) claudin-2 (green) and (d) JAM-A (red) with DAPI nuclear counterstain (blue). Quantification of confocal micrographs show that (e) claudin-2 coverage increases on eECM with decreased CBD density and decreased stiffness and that (f) JAM-A distribution remains unchanged. *$p < 0.05$, **$p < 0.01$, ***$p < 0.001$. "n.s." denotes not statistically significant with $p > 0.05$. (For interpretation of the references to colour in this figure legend, the reader is referred to the web version of this article.)

naproxen compared to dexamethasone. Paracellularly transported compounds famotidine [67], ranitidine [62], nadolol [12], and atenolol [64] are absorbed at rates of 35%, 51%, 45%, and 50% *in vivo*, respectively. The P_{app} values of famotidine, ranitidine, and atenolol scale in approximately the same way that dexamethasone and naproxen scale with *in vivo* absorption, though the P_{app} value

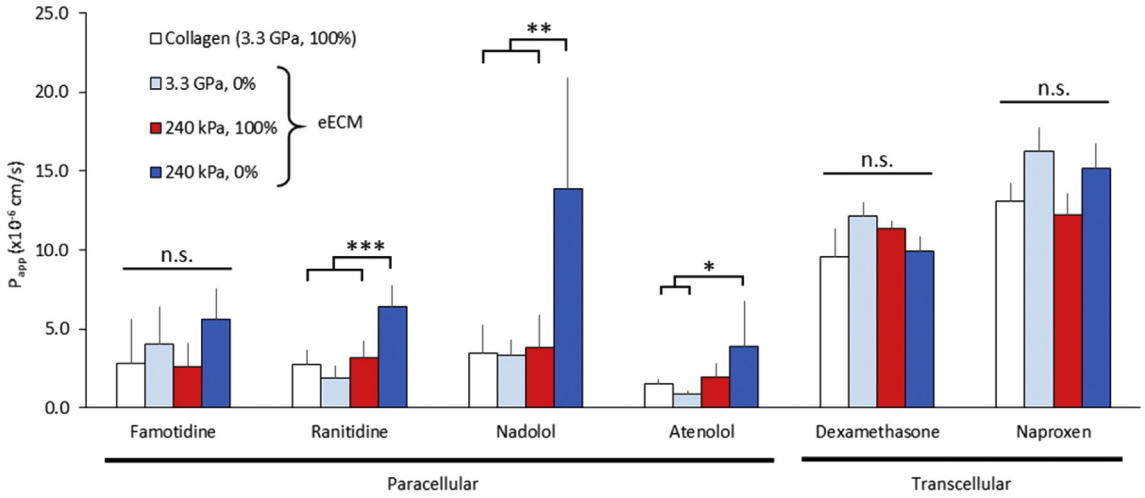

Fig. 6. Apparent permeability, P_{app}, of a variety of paracellularly and transcellularly transported drugs. In general, paracellular transport was increased for cells on eECM with decreased CBD and decreased stiffness, while transcellular transport was unaffected. Caco-2 cells demonstrated enhanced P_{app} of the paracellularly absorbed ranitidine (Zantac®), nadolol (Corgard®), and atenolol (Tenormin®). No difference in transport was observed for transcellularly absorbed dexamethasone (Decadron®) and naproxen (Aleve®). *$p < 0.05$, **$p < 0.01$, ***$p < 0.001$.

obtained for nadolol deviates from this relationship, reflecting the high variability in measurements that can be observed in the Caco-2 model.

The substitution of an eECM for adsorbed collagen I in the Caco-2 assay represents a facile modification to this system that has the potential to further improve the physiological accuracy of this model of oral drug absorption. As such, it is amenable to incorporation into current high-throughput preclinical drug screening performed by the pharmaceutical industry.

3. Conclusions

We have demonstrated the capacity of eECM biomaterials to affect the paracellular permeability of mature Caco-2 monolayers via control of CBD density and mechanical stiffness. By independently tuning these two parameters, we found that increased permeability was observed across Caco-2 monolayers that were cultured on matrices with decreased CBD density and lower mechanical stiffness. The independent tuning of these two matrix parameters was made possible through the engineering of modular peptide domains derived from fibronectin and elastin. These changes in cell-matrix interaction resulted in control of cell spreading, apical actin organization, and expression of the barrier-weakening, tight junction protein claudin-2. Overall, these data demonstrate that careful design of biomaterials can be used to modify cell-cell junctions through control of cell-matrix adhesions and the resulting cytoskeletal tension. This general concept may be useful in the design of biomaterial substrates for other applications that require control over cell-cell junctions.

Specifically, by simply replacing the standard collagen I substrate with a compliant, low cell-adhesive eECM, we significantly improved the paracellular transport rate of drugs within this model without adversely affecting transcellular transport.

4. Materials and methods

4.1. eECM and collagen substrate fabrication

Recombinant eECM proteins were coded into pET15b plasmids under the control of a T7 promoter, expressed in BL21(DE3) *Escherichia coli*, and purified through iterative thermal cycling as previously described [46]. Purified eECM was solubilized in phosphate buffered saline (PBS) overnight at 4 °C prior to use. All protein substrates (eECM or collagen) were fabricated on porous polycarbonate (PC) membranes of constant stiffness and thickness, similar to those used in the standard Caco-2 assay. To generate crosslinked coatings, eECM was covalently crosslinked to form hydrogels on 24-well polycarbonate (PC) transwell inserts (EMD Millipore) using tetrakis (hydroxymethyl) phosphonium chloride, THPC (Sigma Aldrich). eECM and THPC were mixed to achieve the desired reactive group stoichiometric ratio with a total volume of 30 μL. The THPC to eECM ratios tested were: 0.5:1 for 240 kPa substrates and 1:1 for 640 kPa substrates. For all substrates, eECM and THPC were mixed and cast evenly on the porous PC membranes, centrifuged at 150 *g* for 3 min at 2 °C, subsequently given 2 h at 4 °C to crosslink and a minimum of 12 h to equilibrate at 37 °C. Samples were then rinsed with PBS, UV-sterilized for 1 h at room temperature, and then rehydrated in PBS for 3 h at 37 °C, prior to use as a culture substrate.

For adsorbed coatings, eECM was solubilized at 1 mg mL^{-1}, while rat tail collagen I (Sigma Aldrich) was diluted to 3 μg mL^{-1}. Protein solutions (500 μL) were added into the transwell inserts and incubated overnight at 37 °C. All eECM and collagen substrates were rinsed 3 times in PBS warmed to 37 °C prior to cell seeding.

4.2. ECM stiffness characterization

Crosslinked coatings of eECM were formed in 24-well transwell inserts as described above. For atomic force microscopy (AFM) measurements, eECM crosslinked coatings were formed on porous PC membranes (EMD Millipore) that were confined to a 10-mm diameter spread area using silicone sheet molds (Electron Microscopy Sciences) to mimic the internal diameter of the 24-well transwell inserts used for the Caco-2 assay. Samples were rehydrated and measured while submerged in PBS. Short silicon contact mode probes (Applied NanoStructures) were used to collect measurements using 1 μm force distance, 1 Hz scanning rate, 0.5 V trigger point, and an internal gain of 10. Data was fit using the Hertz indentation model for a cone-tip geometry, assuming a Poisson ratio of 0.4.

4.3. Caco-2 culture

Caco-2 cells (ATCC, passages between 15 and 40) were seeded onto prepared substrates at 10^4 cells cm^{-1} and cultured in phenol red-free Dulbecco's Modified Eagle's Media (DMEM) supplemented with 20% fetal bovine serum (FBS), 1% L-glutamine, and 1% penicillin-streptomycin (Thermo Fisher Scientific) at 37 °C, 5% CO_2. 400 μL of media was added into the transwell inserts and 600 μL into the outer well, with care not to disturb the membrane. Media was changed every 3–4 days, and total culture time ranged from 24 to 28 days to allow for mature, polarized monolayer formation.

4.4. Immunocytochemistry

All solutions were made in 1X Dulbecco's PBS, DPBS (Thermo Fisher Scientific), unless otherwise noted. Caco-2 monolayers were fixed in 4% paraformaldehyde (PFA, Electron Microscopy Sciences) quenched in 0.1 M glycine for 30 min, washed in DPBS, permeabilized in 0.2% Triton-X 100 (Sigma Aldrich) for 1 h, washed in DPBS, blocked in 1.5% heat-shocked BSA (Roche) for 3 h, washed in DPBS, and then incubated in primary antibody diluted in 1.5% heat-shocked BSA (Roche) for 2 h at 4 °C. Samples were then rinsed twice in 0.2% Triton-X 100 (Sigma Aldrich), once in DPBS, and incubated in secondary antibody diluted in 1.5% heat-shocked BSA (Roche) for 2 h at room temperature. Samples were then rinsed twice in 0.2% Triton-X 100 (Sigma Aldrich) and once in DPBS. PC membranes were removed from the transwell inserts and mounted onto glass coverslips using 10 μL of ProLong Gold Antifade Reagent (Thermo Fisher Scientific). Images were acquired on a confocal microscope (Leica). The following primary antibodies and stains were used according to manufacturers' suggested dilutions: claudin-2 (Abcam), JAM-A and rhodamine-phalloidin (Sigma Aldrich), and 4′,6-diamidino-2-phenylindole (DAPI, Thermo Fisher Scientific). Claudin-2 primary antibodies were labeled with Alexa Fluor 488 anti-rabbit secondary antibodies (Thermo Fisher Scientific) diluted at 1:500. JAM-A primary antibodies were labeled with Alexa Fluor 647 anti-mouse secondary antibodies (Thermo Fisher Scientific) diluted at 1:500.

4.5. Scanning electron microscopy (SEM)

Primary murine small intestinal tissue samples were derived from adult C57BL/6 mice (Jackson Laboratories). Entire lengths of small intestine were isolated using aseptic techniques, and the lumen was flushed with ice-cold PBS containing 1% penicillin/streptomycin supplementation (Life Technologies) using a syringe needle to remove any remaining contents.

Caco-2 monolayers and primary murine tissue were fixed in 4% PFA (Electron Microscopy Sciences) for 30 min and overnight, respectively. Primary tissue samples were then treated with 1% OsO_4 for 1 h. All samples were rinsed twice in water and sequentially dehydrated in 30%, 50%, 70%, 90%, and 100% ethanol for 10 min each. After another 10-min incubation in 100% ethanol, samples were critical point dried (Tousimis), coated with 10 nm-thick Au/Pd (Denton Vacuum), and then imaged with a variable pressure scanning electron microscope (Hitachi).

Projected cell area was calculated using the particle analysis tool after first tracing cell outlines using Fiji, both on ImageJ (NIH). Only cells whose boundaries were completely within the field of view were considered.

4.6. Flow cytometry

Caco-2 cells were dissociated from tissue culture polystyrene using 0.25% trypsin with 1 mM ethylenediaminetetraacetic acid (EDTA, Thermo Fisher Scientific), centrifuged at 500 *g* for 4 min at room temperature, rinsed in PBS, and then resuspended in integrin binding buffer (25 mM Tris pH 7.4, 150 mM NaCl, 2 mM $CaCl_2$, 1 mM $MgCl_2$, 1 mM $MnCl_2$, 0.1% BSA) at 2×10^5 cells per staining reaction. Integrin-binding antibody was added into each reaction at 1:25, and allowed to incubate for 40 min at 4 °C in the dark. Cells were centrifuged as above, rinsed with 1 mL of integrin binding buffer, and run on a flow cytometer (EMD Millipore). Data analyses was performed using the FlowJo software (Tree Star). The following integrin-binding antibodies were used: FITC-anti-CD49e, FITC-anti-CD51, FITC-anti-CD51/61, AlexaFluor488-anti-CD29, PE-anti-β_5 (BioLegend), and AlexaFluor488-anti-$\alpha_v\beta_5$ (Abcam). Data were analyzed relative to isotype controls.

4.7. Inulin-FITC and drug transport studies

After 24–28 days of culture, medium containing molecules of interest were added into the internal compartment of a transwell insert containing mature Caco-2 monolayers and incubated for 2 h at 37 °C, 5% CO_2. Medium from the basal compartment was then collected and used to measure apparent permeability, P_{app}, according to the following equation:

$$P_{app} = \frac{dQ/dt}{S \cdot C_0}$$

where S is the monolayer surface area, C_0 is the initial apical concentration, and dQ/dt is the temporal mass flow into basal compartment. Inulin-FITC (Sigma Aldrich), famotidine (Tokyo Chemical Industry), nadolol (Sigma Aldrich), and atenolol (Sigma Aldrich) were added at 100 μM initial concentrations. Ranitidine (Tokyo Chemical Industry) and naproxen (Enzo) were added at 300 μM initial concentrations, and dexamethasone was added at 10 μM initial concentration. Standard curves were generated through serial dilutions in Caco-2 conditioned media.

To validate the transport model, inulin-FITC concentration was measured on a fluorescence plate reader (Molecular Devices). To verify the linearity of the transport of this molecule over time on collagen and our eECM substrates, samples were removed from the basolateral side of the transwell insert, at time points ranging from 1 to 24 h. After each sample was taken, equivalent amounts of fresh medium were added back to the basolateral compartment, so as not to introduce bulk fluid flow imbalance into the system. Similar to the published protocols of others, a time point of 2 h was chosen for comparison across all drugs and all conditions.

All other drugs were analyzed via liquid chromatography-mass spectrometry, LC-MS (Agilent), prior to which excess protein and lipid were removed from the basal media using the plasma crash method. Briefly, samples were centrifuged at 16,100 *g* for 1 h at room temperature, diluted 4× in cold acetonitrile, incubated overnight at 4 °C, and centrifuged again at 16,100 *g* for 1 h at 4 °C. The supernatant was collected and centrifuged at 16,100 *g* for 1 h at room temperature. The cleared samples were collected and stored at 4 °C until processing. Immediately prior to running on the LC-MS, samples were centrifuged at 16,100 *g* for 1 h at room temperature to ensure sample clarity.

4.8. Fluorescent image analysis

Confocal images of nuclear staining (DAPI) were analyzed using ImageJ (NIH) to determine the number of cells contained within a fully formed monolayer. For every condition, 3 distinct areas were analyzed on each of 6 individual inserts, for a total of 18 images. Image window sizes were 550 μm × 550 μm (302,500 μm^2). The particle analysis tool determined the number of nuclei in each

image. Total area divided by the number of nuclei was used to calculate the average cell-spread area.

Junctional accumulation of actin was analyzed on a per cell basis. Single-slice confocal images of the apical junctions were taken at the z-plane where the junctional actin ring was most visible. Images were thresholded at 95% of the mean pixel intensity. The fraction of positively stained pixels was converted to an area and divided by the cell count within that image, as determined by DAPI nuclear staining. A minimum of 5 images was analyzed per condition.

Claudin-2 and JAM-A confocal images were analyzed to assess the percent area of coverage per image. Images were first thresholded at a constant intensity cutoff value followed by application of the ImageJ "Despeckle" command. Percent area of the image that was positively labeled for claudin-2 expression was then quantified. A minimum of three images per condition was analyzed.

4.9. Quantitative real-time PCR (qRT-PCR)

RNA was isolated from mature Caco-2 monolayers after 24–28 days of culture using Trizol reagent (Thermo Fisher Scientific) and phase-lock gels (5 PRIME), according to manufacturers' instructions. cDNA was generated from 1 μg of RNA using the High Capacity Reverse Transcription Kit (Applied Biosystems), and qRT-PCR performed using SYBR Green on a StepOnePlus platform (Applied Biosystems) with 18S as endogenous control. Sequences of forward and reverse primers are found in the Supplemental Information (Table S1).

Quantification of relative expression of RNA by RT-PCR was performed by the "Comparative C_T Method" with 18S as the internal control and values reported relative to that for cells on adsorbed collagen.

4.10. Statistical analyses

All statistical analyses were performed using Prism (GraphPad). Unless otherwise indicated, data are displayed as mean ± standard deviation (SD), and statistical significance were calculated between groups using a one-way ANOVA followed by a Tukey *post-hoc* test.

Acknowledgments

The authors gratefully acknowledge funding from the National Institutes of Health R21 EB018407 and U19 AI116484 (SCH). The authors thank the Cell Sciences Imaging Facility at Stanford University for providing access to scanning electron microscopy. Thanks to the laboratory of Prof. Elizabeth Sattely as well as Dr. Jakub Rajniak for use and assistance in liquid chromatography-mass spectrometry. The authors further acknowledge the laboratories of Prof. Jennifer Cochran for access to flow cytometry equipment, and Prof. Nicholas Melosh for use of atomic force microscopy equipment. Thanks to the laboratory of Prof. Calvin Kuo for assistance in obtaining primary murine small intestinal tissue samples.

Appendix A. Supplementary data

Supplementary data related to this article can be found at http://dx.doi.org/10.1016/j.biomaterials.2017.03.023.

References

[1] E.H. Moeller, L. Jorgensen, Alternative routes of administration for systemic delivery of protein pharmaceuticals, Drug Discov. Today Technol. 5 (2009).
[2] Y. Masaoka, Y. Tanaka, M. Kataoka, S. Sakuma, S. Yamashita, Site of drug absorption after oral administration: assessment of membrane permeability and luminal concentration of drugs in each segment of gastrointestinal tract, Eur. J. Pharm. Sci. 29 (2006) 240–250.
[3] N. Ward, The impact of intestinal failure on oral drug absorption: a Review, J. Gastrointest. Surg. 14 (2010) 1045–1051.
[4] M.J. Cho, D.P. Thompson, C.T. Cramer, T.J. Vidmar, J.F. Scieszka, The Madin Darby canine kidney (MDCK) epithelial cell monolayer as a model cellular transport barrier, Pharm. Res. Off. J. Am. Assoc. Pharm. Sci. 6 (1989) 71–77.
[5] J.D. Irvine, et al., MDCK (Madin-Darby canine kidney) cells: a tool for membrane permeability screening, J. Pharm. Sci. 88 (1999) 28–33.
[6] C.B. Collares-Buzato, M.A. Jepson, G.T.A. McEwan, B.H. Hirst, N.L. Simmons, Co-culture of two MDCK strains with distinct junctional protein expression: a model for intercellular junction rearrangement and cell sorting, Cell Tissue Res. 291 (1998) 267–276.
[7] D.A. Volpe, Variability in caco-2 and MDCK cell-based intestinal permeability assays, J. Pharm. Sci. 97 (2008) 712–725.
[8] J.W. Polli, et al., Rational use of in vitro P-glycoprotein assays in drug discovery, J. Pharmacol. Exp. Ther. 299 (2001) 620–628.
[9] I.J. Hidalgo, T.J. Raub, R.T. Borchardt, Characterization of the human colon carcinoma cell line (Caco-2) as a model system for intestinal epithelial permeability, Gastroenterology 96 (1989) 736–749.
[10] Y. Sambuy, et al., The Caco-2 cell line as a model of the intestinal barrier: influence of cell and culture-related factors on Caco-2 cell functional characteristics, Cell Biol. Toxicol. 21 (2005) 1–26.
[11] P. Shah, V. Jogani, T. Bagchi, A. Misra, Role of Caco-2 cell monolayers in prediction of intestinal drug absorption, Biotechnol. Prog. 22 (2006) 186–198.
[12] N. Li, et al., Development of an improved three-dimensional *in vitro* intestinal Mucosa model for drug absorption evaluation, Tissue Eng. Part C Methods 19 (2013) 708–719.
[13] H. Sun, E.C.Y. Chow, S. Liu, Y. Du, K.S. Pang, The Caco-2 cell monolayer: usefulness and limitations, Expert Opin. Drug Metab. Toxicol. 4 (2008) 395–411.
[14] L.S. Gan, P.H. Hsyu, J.F. Pritchard, D. Thakker, Mechanism of intestinal absorption of ranitidine and ondansetraon: transport across Caco-2 cell monolayers, Pharm. Res. 10 (1993) 1722.
[15] A. van Hecken, T. Tjandramaga, A. Mullie, R. Verbesselt, P. De Schepper, Ranitidine: single dose pharmacokinetics and absolute bioavailability in man, Br. J. Clin. Pharmacol. 14 (1982) 195–200.
[16] A. Merzlikine, et al., Effect of chitosan glutamate, carbomer 974P, and EDTA on the in vitro Caco-2 permeability and oral pharmacokinetic profile of acyclovir in rats, Drug Dev. Ind. Pharm. 35 (2009) 1082–1091.
[17] L. Peng, Z. He, W. Chen, I.R. Holzman, J. Lin, Effects of butyrate on intestinal barrier function in a caco-2 cell monolayer model of intestinal barrier, Pediatr. Res. 61 (2007) 37–41.
[18] D.S. Cox, S. Raje, H. Gao, N.N. Salama, N.D. Eddington, Enhanced permeability of molecular weight markers and poorly bioavailable compounds across Caco-2 cell monolayers using the absorption enhancer, zonula occludens toxin, Pharm. Res. 19 (2002) 1680–1688.
[19] L.W. Hsu, et al., Effects of pH on molecular mechanisms of chitosan-integrin interactions and resulting tight-junction disruptions, Biomaterials 34 (2013) 784–793.
[20] L.W. Hsu, et al., Elucidating the signaling mechanism of an epithelial tight-junction opening induced by chitosan, Biomaterials 33 (2012) 6254–6263.
[21] C. Hilgendorf, H. Spahn-langguth, C.G. Regårdh, E. Lipka, Caco-2 versus Caco-2/HT29-MTX Co-cultured cell lines: permeabilities via diffusion, inside- and outside-directed carrier-mediated transport, J. Pharm. Sci. 89 (2000) 63–75.
[22] H. Satsu, T. Yokoyama, N. Ogawa, Y. Fujiwara-Hatano, M. Shimizu, Effect of neuronal PC12 cells on the functional properties of intestinal epithelial Caco-2 cells, Biosci. Biotechnol. Biochem. 67 (2003) 1312–1318.
[23] S.M. Moyes, J.F. Morris, K.E. Carr, Macrophages increase microparticle uptake by enterocyte-like Caco-2 cell monolayers, J. Anat. 217 (2010) 740–754.
[24] E. Walter, S. Janich, B.J. Roessler, J.M. Hilfinger, G.L. Amidon, HT29-MTX/Caco-2 cocultures as an in vitro model for the intestinal epithelium: in vitro-in vivo correlation with permeability data from rats and humans, J. Pharm. Sci. 85 (1996) 1070–1076.
[25] T. Mizutani, et al., Real-time analysis of P-glycoprotein-mediated drug transport across primary intestinal epithelium three-dimensionally cultured in vitro, Biochem. Biophys. Res. Commun. 419 (2012) 238–243.
[26] J. Zhao, et al., A novel model of P-Glycoprotein inhibitor screening using human small intestinal organoids, Basic Clin. Pharmacol. Toxicol. (2016), http://dx.doi.org/10.1111/bcpt.12680.
[27] H.J. Kim, D.E. Ingber, Gut-on-a-Chip microenvironment induces human intestinal cells to undergo villus differentiation, Integr. Biol. 5 (2013) 1130.
[28] Y. Ma, et al., Focal adhesion kinase regulates intestinal epithelial barrier function via redistribution of tight junction, Biochim. Biophys. Acta 1832 (2013) 151–159.
[29] W. Ziegler, A. Gingras, D. Critchley, J. Emsley, Integrin connections to the cytoskeleton through talin and vinculin, Biochem. Soc. Trans. 36 (2008) 235–239.
[30] M.P. Playford, K. Vadali, X. Cai, K. Burridge, M.D. Schaller, Focal Adhesion Kinase regulates cell-cell contact formation in epithelial cells via modulation of Rho, Exp. Cell Res. 314 (2008) 3187–3197.
[31] T.Y. Ma, et al., Cytoskeletal regulation of Caco-2 intestinal monolayer paracellular permeability, J. Cell Physiol. 164 (1995) 533–545.
[32] B.C. Elias, et al., The integrin??1 subunit regulates paracellular permeability of kidney proximal tubule cells, J. Biol. Chem. 289 (2014) 8532–8544.

[33] P.K. Nighot, et al., Matrix Metalloproteinase 9-induced increase in intestinal epithelial tight junction permeability contributes to the severity of experimental DSS colitis, Am. J. Physiol. Gastrointest. Liver Physiol. (2015), http://dx.doi.org/10.1152/ajpgi.00256.2015 ajpgi.00256.2015.
[34] S.-T. Sit, E. Manser, Rho GTPases and their role in organizing the actin cytoskeleton, J. Cell Sci. 124 (2011) 679–683.
[35] D. Spiering, L. Hodgson, Dynamics of the rho-family small GTPases in actin regulation and motility, Cell Adhes. Migr. 5 (2011) 170–180.
[36] A. Engler, et al., Substrate compliance versus ligand density in cell on gel response, Biophys. J. 86 (2004) 617–628.
[37] K. Saha, E.F. Irwin, J. Kozhukh, D.V. Schaffer, K.E. Healy, Biomimetic interfacial interpenetrating polymer networks control neural stem cell behavior, J. Biomed. Mater. Res. - Part A 81 (2007) 240–249.
[38] U.S. Schwarz, M.L. Gardel, United we stand - integrating the actin cytoskeleton and cell-matrix adhesions in cellular mechanotransduction, J. Cell Sci. 125 (2012) 3051–3060.
[39] B. Geiger, J.P. Spatz, A.D. Bershadsky, Environmental sensing through focal adhesions, Nat. Rev. Mol. Cell Biol. 10 (2009) 21–33.
[40] S. Chen, R. Einspanier, J. Schoen, Transepithelial electrical resistance (TEER): a functional parameter to monitor the quality of oviduct epithelial cells cultured on filter supports, Histochem. Cell Biol. 144 (2015) 509–515.
[41] S. Yuan, R. Rigor, in: Regulation of Endothelial Barrier Function, 2010, pp. 1–14 doi:2011.
[42] Z. Liu, K. Liu, The transporters of intestinal tract and techniques applied to evaluate interactions between drugs and transporters, Asian J. Pharm. Sci. 8 (2013) 151–158.
[43] F. Gao, D. Liao, A.M. Drewes, H. Gregersen, Modelling the elastin, collagen and smooth muscle contribution to the duodenal mechanical behaviour in patients with systemic sclerosis, Neurogastroenterol. Motil. 21 (2009).
[44] L. Wang, S.K. Murthy, G.A. Barabino, R.L. Carrier, Synergic effects of crypt-like topography and ECM proteins on intestinal cell behavior in collagen based membranes, Biomaterials 31 (2010) 7586–7598.
[45] J.C. Liu, S.C. Helishorn, D.A. Tirrell, Comparative cell response to artificial extracellular matrix proteins containing the RGD and CS5 cell-binding domains, Biomacromolecules 5 (2004) 497–504.
[46] K.S. Straley, S.C. Heilshorn, Independent tuning of multiple biomaterial properties using protein engineering, Soft Matter 5 (2009) 114.
[47] A. Buxboim, I.L. Ivanovska, D.E. Discher, Matrix elasticity, cytoskeletal forces and physics of the nucleus: how deeply do cells 'feel' outside and in? J. Cell Sci. 123 (2010) 297–308.
[48] D.A.K. Watters, A.N. Smith, M.A. Eastwood, K.C. Anderson, R.A. Elton, Mechanical properties of the rat colon: the effect of age, sex and different conditions of storage, Q. J. Exp. Physiol. 70 (1985) 151–162.
[49] R. Roeder, et al., Compliance, elastic modulus, and burst pressure of small-intestine submucosa (SIS), small-diameter vascular grafts, J. Biomed. Mater. Res. 47 (1999) 65–70.
[50] Y. Leng, Z. Ding, L. Gong, Elastic modulus of small intestinal submucosa, Zhongguo Xiu Fu Chong Jian Wai Ke Za Zhi 20 (2006) 292–294.
[51] C. Chung, K.J. Lampe, S.C. Heilshorn, Tetrakis(hydroxymethyl) phosphonium chloride as a covalent cross-linking agent for cell encapsulation within protein-based hydrogels, Biomacromolecules 13 (2012) 3912–3916.
[52] A.P. Mould, J.A. Askari, M.J. Humphries, Molecular basis of ligand recognition by integrin alpha5beta1, J. Biol. Chem. 275 (2000) 20324–20336.
[53] J.F. Marshall, et al., Alpha v beta 1 is a receptor for vitronectin and fibrinogen, and acts with alpha 5 beta 1 to mediate spreading on fibronectin, J. Cell Sci. 108 (1995) 1227–1238.
[54] Z. Zhang, K. Vuori, J.C. Reed, E. Ruoslahti, The alpha 5 beta 1 integrin supports survival of cells on fibronectin and up-regulates Bcl-2 expression, Proc. Natl. Acad. Sci. U. S. A. 92 (1995) 6161–6165.
[55] Y. Takada, X. Ye, S. Simon, The integrins, Genome Biol. 8 (2007) 215.
[56] P.L. Benitez, S. Mascharak, A.C. Proctor, S. Heilshorn, Use of protein-engineered fabrics to identify design rules for integrin ligand clustering in biomaterials, Integr. Biol. 8 (2015) 50–61.
[57] S.J. Terry, et al., Spatially restricted activation of RhoA signalling at epithelial junctions by p114RhoGEF drives junction formation and morphogenesis, Nat. Cell Biol. 13 (2011) 159–166.
[58] G. Ranaldi, I. Marigliano, I. Vespignani, G. Perozzi, Y. Sambuy, The effect of chitosan and other polycations on tight junction permeability in the human intestinal Caco-2 cell line(1), J. Nutr. Biochem. 13 (2002) 157–167.
[59] T. Shiobara, T. Usui, J. Han, H. Isoda, Y. Nagumo, The reversible increase in tight junction permeability induced by capsaicin is mediated via cofilin-actin cytoskeletal dynamics and decreased level of occludin, PLoS One 8 (2013).
[60] F. Escaffit, F. Boudreau, J.F. Beaulieu, Differential expression of claudin-2 along the human intestine: implication of GATA-4 in the maintenance of claudin-2 in differentiating cells, J. Cell. Physiol. 203 (2005) 15–26.
[61] J.E. de Vries, et al., Human Caco-2 cells transfected with c-Ha-Ras as a model for endocrine differentiation in the large intestine, Differentiation. 53 (1993) 51–60.
[62] K. Lee, D.R. Thakker, Saturable transport of H2-antagonists ranitidine and famotidine across Caco-2 cell monolayers, J. Pharm. Sci. 88 (1999) 680–687.
[63] H. Lennernas, O. Ahrenstedt, A. Ungell, Intestinal drug absorption during induced net water absorption in man; a mechanistic study using antipyrine, atenolol and enalaprilat, Br. J. Clin. Pharmacol. 37 (1994) 589–596.
[64] P. Artursson, J. Karlsson, Correlation between oral drug absorption in humans and apparent drug permeability coefficients in human intestinal epithelial (Caco-2) cells, Biochem. Biophys. Res. Comm. 175 (1991) 880–885.
[65] A. El-Kattan, M. Varma, Oral absorption, intestinal metabolism and human oral bioavailability, Top. Drug Metab. (2005) 1–35, http://dx.doi.org/10.5772/31087.
[66] V. Pade, S. Stavchansky, Link between drug absorption solubility and permeability measurements in Caco-2 cells, J. Pharm. Sci. 87 (1998) 1604–1607.
[67] J.H. Lin, Pharmacokinetic and pharmacodynamic properties of histamine H2-Receptor antagonists: relationship between intrinsic potency and effective plasma concentrations, Clin. Pharmacokinet. 20 (1991) 218–236.